Cooperative Phenomena Driven by Spin-Orbit Interaction and Magnetism

The spin-orbit interaction (SOI) and magnetism are closely related to each other. The magnetic structure is modified by the SOI, whose famous examples are the weak ferromagnetism and helical magnetism due to the Dzyaloshinsky-Moriya (DM) interaction. Also, transport phenomena are affected both by the SOI and magnetism. The spin Hall effect (SHE) and topological insulators (TIs) are examples of the phenomena driven by the SOI, and the anomalous Hall effect (AHE) is a very phenomenon which results from the combination of the SOI and magnetism. In the present Ph. D. Thesis, we focus on such cooperative phenomena driven by the SOI and magnetism.

In Chapter 1, we briefly introduce the SOI and magnetism, respectively, and a few examples where the SOI and magnetism coexist. First we review our previous work on a TI in a $5d$ transition metal oxide Na_2IrO_3. In this material, the SOI and electronic interaction have the similar energy scale. We performed the first-principles band calculations and derived the tight-binding model, which is found to have the non-trivial Z_2 topological invariant. Next we introduce the semiconductor quantum dot (QD) system, which is studied in Chapter 2. Usually in semiconductors, the SOI is relevant while magnetism induced by the electronic interaction does not matter. However, when a few electrons are confined in a small region of QDs, their spin degrees of freedom show up and can be manipulated by the SOI. Finally we introduce the AHE, which is the subject of Chapter 3. It is a phenomenon in which the transverse charge current is produced due to the SOI in ferromagnets.

In Chapter 2, we theoretically propose how to manipulate electron spins without magnetic field or magnets in a double QD. We consider the exchange and time-dependent DM interactions,

$$H(t) = J(\vec{s}_1 \cdot \vec{s}_2 - 1/4) + \vec{D}(t) \cdot \vec{s}_1 \times \vec{s}_2,$$

where the latter arises from the Rashba SOI modulated by electric field. Within the perturbation theory, we analytically construct three unitary operations,

(a) the spin initialization from the singlet ground state to any triplet states,

(b) the two-spin rotations in the opposite directions,

(c) the two-spin rotations in the same direction.

Especially combination of the operations (b) and (c) leads to the one-spin rotations by any angles in any directions, as shown in Fig. 1. Thus we implement the universal quantum gates, which are necessary for quantum computation, only by the electric field. These are confirmed by numerical calculations in which the time-dependent DM interaction is exactly treated and relaxation due to the hyperfine interaction with nuclear spins is included. Here the relaxation terms in the equation of motion of the density matrix are derived by the standard boson-bath

model within the Born-Markov approximation. We propose the experimental setup to generate the three-dimensional electric field necessary for the one-spin rotations, and discuss the realistic time scales of the operations and relaxation.

In Chapter 3, the AHE is numerically studied including the elastic scattering by disorder and the inelastic scattering at finite temperature. Though three mechanisms of the AHE, i.e., the intrinsic mechanism, skew scattering, and side jump, have been unified by the perturbation theory with respect to the disorder at zero temperature, the effects of the inelastic scattering by phonons and magnons at finite temperature remain to be revealed. To study this problem, we consider a fully polarized multiband tight-binding Hamiltonian which shows both the intrinsic and extrinsic mechanisms,

$$
H = -t_0 \sum_{\langle ij \rangle} c_i^\dagger c_j + \epsilon_1 \sum_i^{\text{random}} s_i^\dagger s_i - V_1 \sum_i^{\text{random}} c_i^\dagger s_i + \text{H.c.}
$$
$$
+ \epsilon_2 \sum_i^{\text{random}} p_i^\dagger p_i - V_2 \sum_{\langle ij \rangle}^{\text{random}} e^{-i\theta_{ij}} c_i^\dagger p_j + \text{H.c.},
$$

where s_i and p_i describes the s and $p^x - ip^y$ orbitals of impurity, and calculate the Hall conductivity and resistivity by the finite temperature Kubo formula with the phenomenological inelastic lifetime. We find the new scaling relations represented by

$$
-\sigma_{xy}(T,\gamma) = \rho_{xy0}^{\text{ext}}(T)\sigma_{xx}^2(T,\gamma) + b(T)
$$
$$
\rho_{xy0}^{\text{ext}}(T) = \alpha(T)\sigma_{xx0}^{-1}(T) + \beta(T)\sigma_{xx0}^{-2}(T),
$$

where σ_{xx0}^{-1} is the elastic scattering contribution to the longitudinal resistivity. The first relation, which separates the Hall conductivity into the extrinsic and intrinsic mechanisms, always holds as seen in Fig. 2(a). Combining the Matthiessen's rule $\rho_{xx}(T,\gamma) = \sigma_{xx0}^{-1}(T)(\gamma+\gamma_0)/\gamma_0$ with the elastic scattering γ_0, the first term describing the extrinsic mechanisms is rapidly suppressed by the inelastic scattering, in other words, the inelastic part of the longitudinal resistivity does not contribute to the extrinsic mechanisms of the Hall resistivity. On the other hand, the intrinsic mechanism is quite robust against the inelastic scattering. The second relation, which separates the extrinsic mechanisms into the skew scattering and side jump, holds only when the band structure is well-defined as shown in Fig. 2(b). The temperature dependence comes from two factors, one is that of the inelastic scattering strength $\gamma = \gamma(T)$, and the other is the Fermi distribution function. The temperature dependence of the extrinsic mechanisms is determined mainly by the former, while that of the intrinsic mechanism is determined by the latter since the inelastic scattering is irrelevant, and is enhanced when the resonant condition of the Berry curvature is satisfied. The effect of the ω-dependence of the electron self-energy due to phonons is also discussed. Our findings correspond to the recent measurements of the anomalous part of the Lorentz ratio $L_{xy}^{\text{A}} = \kappa_{xy}^{\text{A}}/\sigma_{xy}^{\text{A}}T$, in which κ_{xy}^{A} is the thermal conductivity.

Chapter 4 is devoted to the concluding remarks.
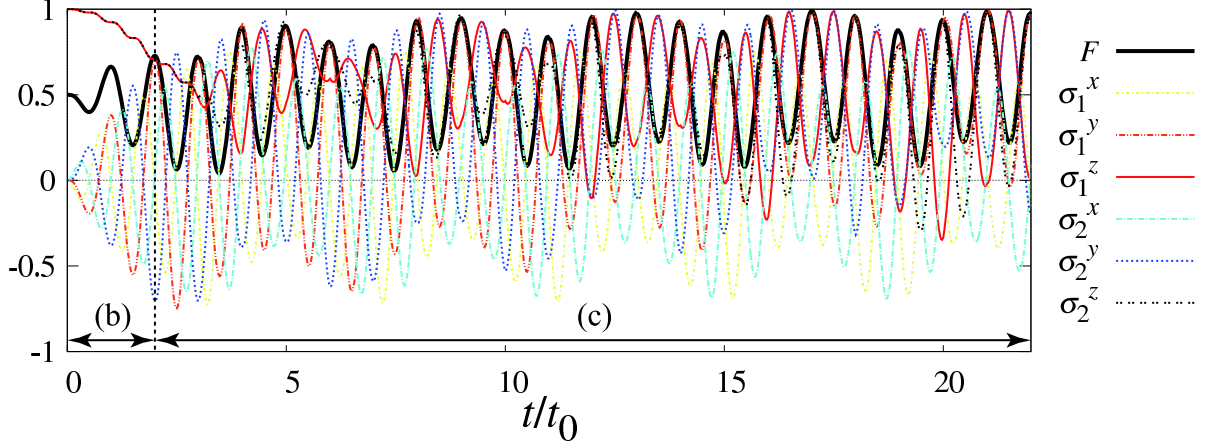
Figure 1: Time evolutions of the fidelity (black line) and spin expectation values in rotation of spin 1 around x axis by $\pi/2$ combined with the operations (b) and (c). The fidelity is defined by $F(t) = [\text{tr} \sqrt{\sqrt{\rho_{\text{fin}}} \rho(t) \sqrt{\rho_{\text{fin}}}}]^2$ with the operated state $\rho(t)$ and the desired final state ρ_{fin}, and satisfies $0 \le F \le 1$ and $F = 1$ for $\rho(t) = \rho_{\text{fin}}$. For simplicity, relaxation is not included.
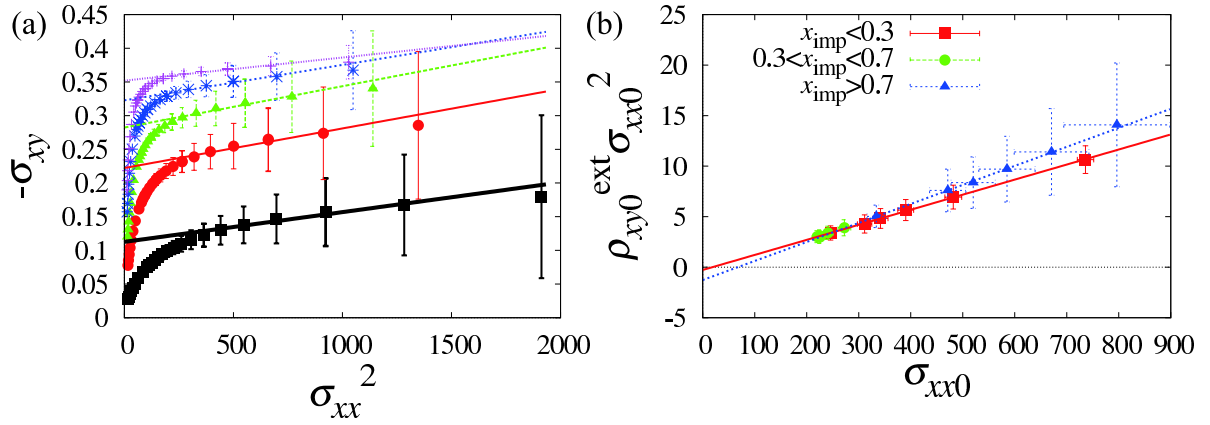
Figure 2: (a) The Hall conductivity $-\sigma_{xy}$ is plotted as a function of σ_{xx}^2 for $x_{\text{imp}} = 0.1$ (black square), 0.3 (red circle), 0.5 (green triangle), 0.7 (blue star), and 0.9 (purple point). (b) Plot for $\rho_{xy0}^{\text{ext}} \sigma_{xx0}^2$ v.s. σ_{xx0}. Lines are obtained by fitting in $x_{\text{imp}} < 0.3$ (red square) and $x_{\text{imp}} > 0.7$ (blue triangle), respectively. Parameters are fixed to $T = 0.3$ and $\mu = \epsilon_2$.